A Dynamic Interpretation of Electron Beam Welding

Oscillation of the cavity formed by the electron beam provides an explanation for weld defects such as spiking, porosity and cracking and provides an explanation for high fusion-zone homogeneity

BY H. TONG AND W. H. GIEDT

Introduction

The deep welding capability of an electron beam has been well publicized by equipment manufacturers as well as independent researchers. In explaining why the depth-to-width ratio of the fusion zone is usually much greater than unity, the existence of a cavity, in the path of the electron beam, has often been postulated. In most cases, analyses are based on a steady state cavity, although the possible unsteady nature of this cavity has often been suggested.[1, 2] The undesirable features of an electron beam weld, such as spikes, cold shuts and base porosity, are often ignored. In many applications where complete penetration of the workpiece is not desired, these defects can lead to premature failure.

H. TONG and W. H. GIEDT are with the Dept. of Mechanical Engineering, College of Engineering, University of California, Davis, Calif.

Paper presented at the AWS 51st Annual Meeting held in Cleveland, Ohio, during June 8-12, 1970.

In attempts to understand how these defects were formed, it appeared as though the formation of the cavity was of primary importance. To verify the existence of a cavity, an experimental program, as described in the literature,[3] was performed. In brief, a pulsed beam of high voltage (about 600 kv) X-rays was passed through a workpiece during the actual welding process so that the size and shape of the cavity were recorded on X-ray film. The X-ray source was not capable of emitting multiple pulses so that only one radiograph was obtained for each bead-on-plate weld pass. This study, which was conducted with a low voltage welding unit (less than 50 kv), not only verified that an electron beam forms a cavity, but probably of greater significance it suggested that the cavity oscillated in size and shape. With this as a background, the present paper proposes a dynamic model for the formation of the cavity and shows how this model accounts for the formation of the aforementioned weld defects.

Experimental Results

Radiographs, showing the cavity, were obtained for bead-on-plate welds on 1100 aluminum and Type 304 stainless steel. Because of the high energy spectrum of the pulsed X-rays, the contrast of the radiographs was generally low so that it was not possible to present these radiographs as results. Instead, artistic representation of typical radiographs are shown in Fig. 1 and 2 for aluminum and stainless steel respectively. It is immediately apparent that the cavity does not have a steady configuration, and since each radiograph is for a different weld pass, there is no relative time base linking the radiographs to each other. Thus if each of the typical cavity shapes represents a different time in one cycle of a near-periodic oscillation, it would be important to know what their appropriate sequence is.

In the analysis to follow, it was necessary to know the approximate size and shape of the molten fluid on the back side of the cavity. This was

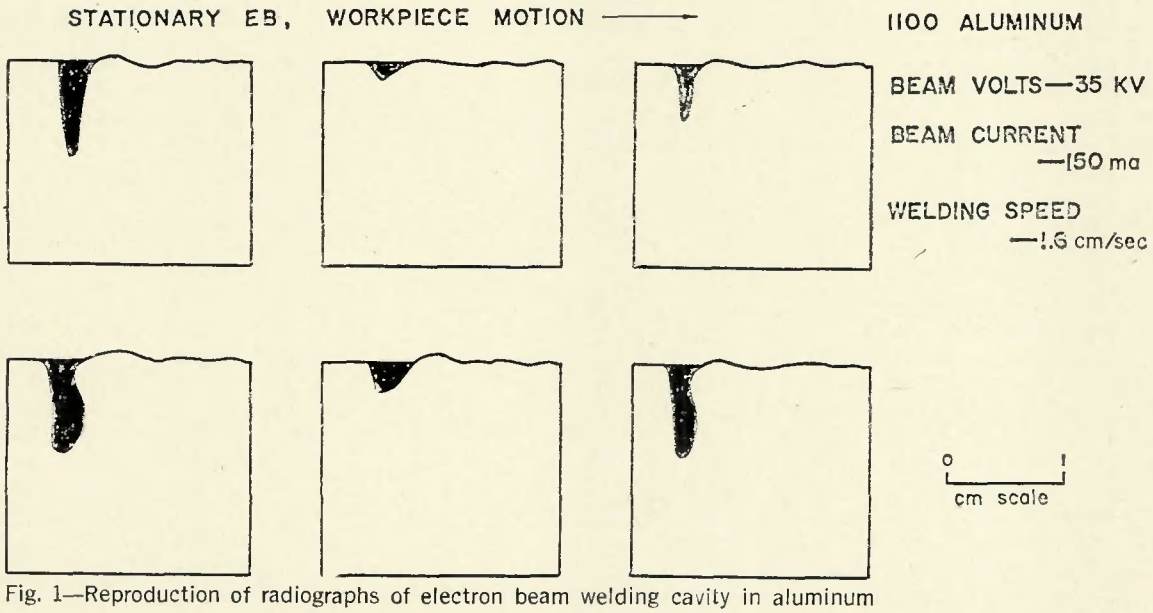

Fig. 1—Reproduction of radiographs of electron beam welding cavity in aluminum

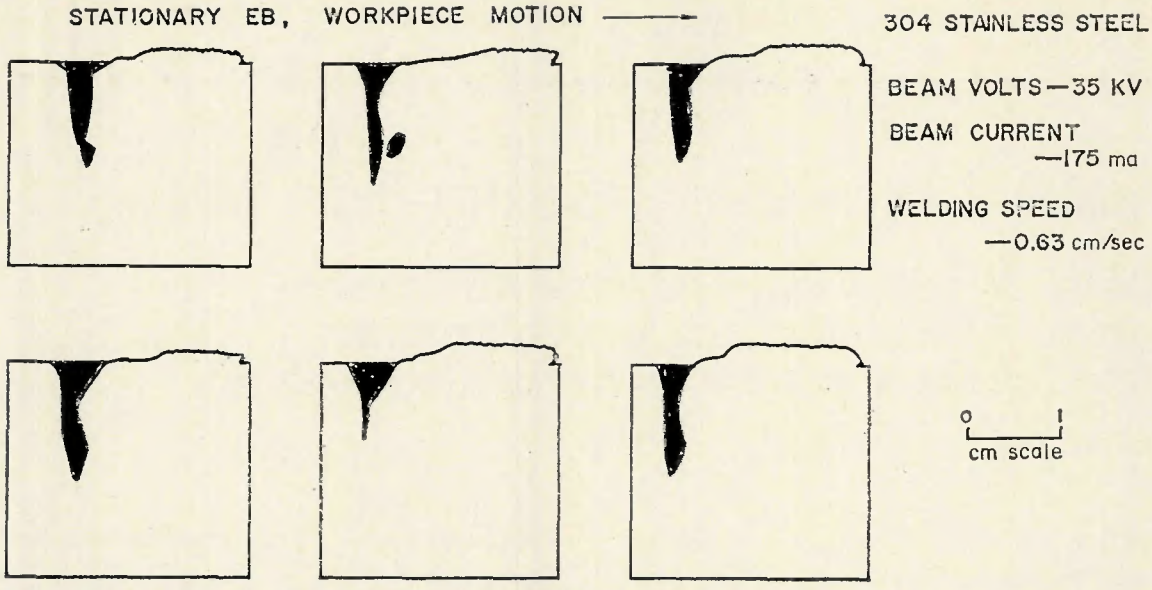

Fig. 2—Reproduction of radiographs of electron beam welding cavity in stainless steel

determined by introducing a local impurity in stainless steel samples as shown in Fig. 3a. A welding pass was then made such that the electron beam cut through the impurity which, due to the motion of the melt, would be distributed throughout the fluid. The samples were subsequently cut, polished, and etched to reveal the pattern shown in Fig. 3b. The outline of the impurity band (the "melt") could be seen and is representative of the back boundary of the melt. By sketching in the approximate shape of the cavity (at maximum penetration), the relative size of the cavity and melt layer can be determined.

Discussion of Experimental Results

Proposed Cavity Oscillation Sequence

The observed characteristic shapes of the cavity bear an amazing similarity to the cavities associated with the entry of projectiles into water. Photographs of the formation of cavities, which form behind spheres[4, 5] and which enter water vertically, show the growth of a cavity, a subsequent necking and closure of the cavity, and establish the difference between surface closure and subsurface closure. Although there are many possible sequences for the radiographs shown in Figs. 1 and 2, the similarity between the shapes of the welding cavity and the cavities shown by Mallock[4] and Gilbarg and Anderson[5] suggests the sequence shown in Figs. 4 and 5.

Consider Fig. 4 which is the proposed cavity oscillation sequence for 1100 aluminum. Note that, even though only the cavity was visible in the radiographs, a melt region was sketched in to give a clearer understanding about the fluctuations of the cavity. The sequence was arbitrarily started with the cavity near its maximum depth. Tracing through the sequence, the cavity is observed to grow laterally near its base possibly due to the high pressures induced by the vaporizing metal, but constricts at a higher location. The melt eventually rolls over or slides into the cavity leaving a large melt region beneath the electron beam and through which the electron beam must once again penetrate. The same general kind of cavity oscillation is seen in Fig. 5 for stainless steel.

The similarity between the water entry phenomena and the development of the electron beam welding cavity makes it possible to draw an analogy between these two phenomena. When

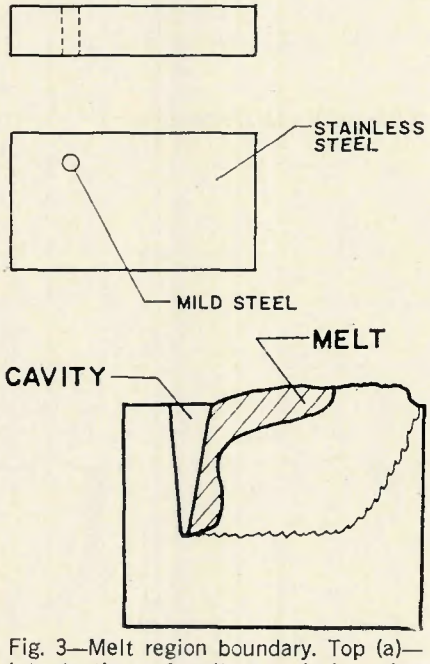

Fig. 3—Melt region boundary. Top (a)—introduction of mild steel impurity; bottom (b)—welding pass pattern

the electron beam strikes the surface of the molten pool, the intense heating causes the material to vaporize and the vapor pressure exerts a downward force on the melt. The vaporizing material creates a hypothetical body which behaves like a projectile and penetrates into the molten metal. This "projectile" continues to penetrate until the hydrostatic forces cause a deep closure or necking of the cavity. This interrupts the electron beam and separates the original cavity into two cavities, a surface cavity and a subsurface cavity. The lower cavity then ceases to penetrate since the driving force (vapor pressure) is removed and this cavity fills with fluid. The inertia of the deep closure causes an upward flow of fluid until it is overcome by the surface vapor pressure and the hypothetical body forms and penetrates again.

The only significant differences between the water entry and electron beam welding cavities are:

1. In the electron beam case, the projectile ceases to penetrate after deep closure occurs.
2. In the electron beam case, the pressure on the inside of the splash is greater than the ambient pressure so that this pressure tends to counteract the surface tension force which is trying to cause surface closure.

It is therefore proposed that the shape of the electron beam welding cavity in this experiment can be considered as being similar to the periodic entry of projectiles into a fluid. Shortly after a deep closure occurs, the electron beam produces the effect of another projectile entering the fluid; the oscillation frequency is thus controlled by the speed of penetration and the fluid properties. The speed of penetration will be controlled primarily by the vapor

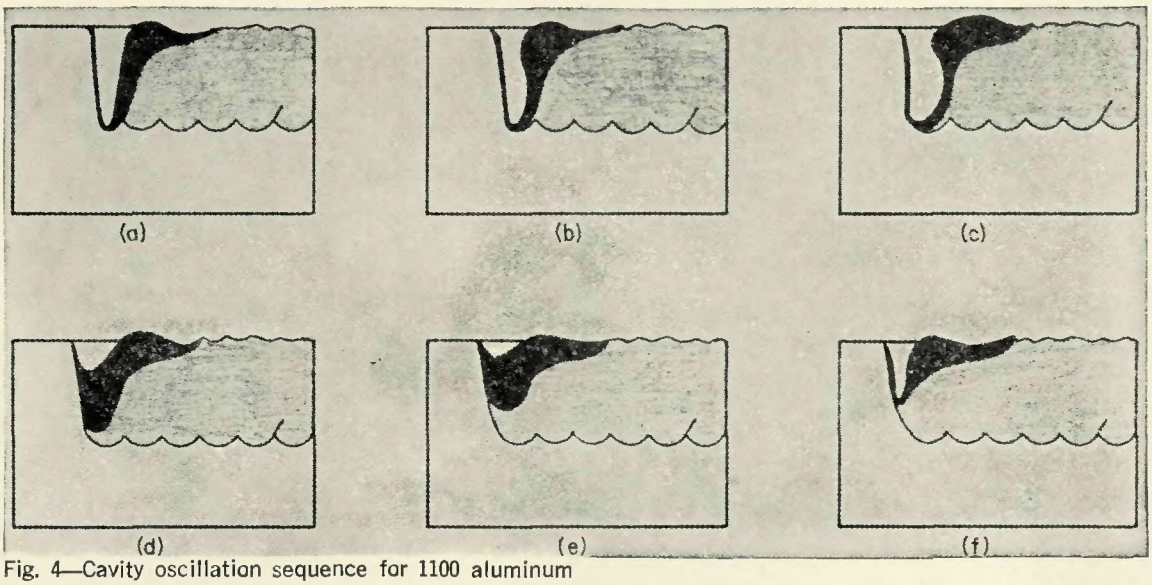

Fig. 4—Cavity oscillation sequence for 1100 aluminum

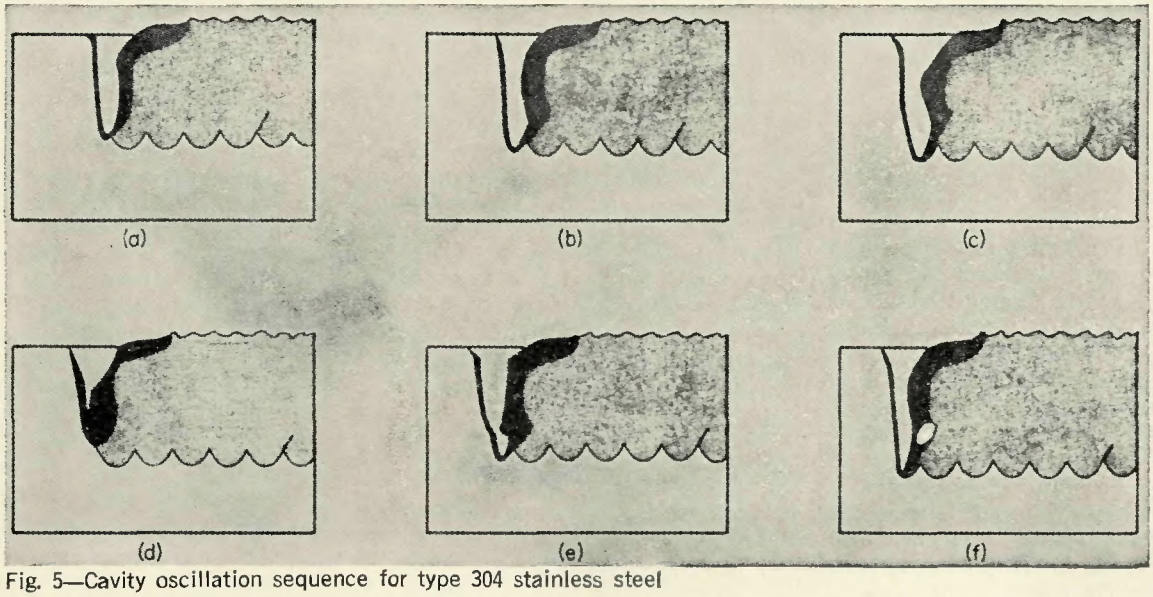

Fig. 5—Cavity oscillation sequence for type 304 stainless steel

pressure (or surface temperature) which will be governed by the electron beam power density.

Fundamental Difference Between Low and High Voltage Welding

Consider the splash shown in Fig. 6. The diameter and height of the splash will be governed principally by the size of the projectile and its entry velocity (assuming a given fluid). Or, analogously, the geometry of the splash will depend on the electron beam spot size and the beam accelerating voltage.

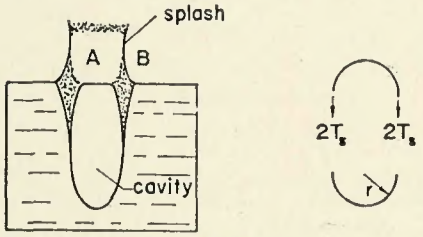

Fig. 6—Formation of splash

The smaller the spot size, the smaller the splash diameter and the greater the beam voltage, the higher the splash. From a gas dynamic standpoint, the static pressure at A cannot be much different from that at B so that the pressure difference is expected to be small but for molten metals the surface tension force is large so that this will be the dominant force tending to close the cavity at the surface. The pressure at A, to prevent surface closure, must be of order $2T_s/r$ where T_s is the surface tension and r is the radius of splash. Thus surface closure is enhanced as r decreases. Since surface closure is not very probable for small splash heights, both higher voltages and smaller spot sizes encourage surface closure.

Thus, low voltage welding is analogous to deep closure as previously described, and high voltage welding is analogous to a combination of surface and deep closure. Since no radiographic studies were made of the latter case, it is not known if the electron beam passes through the surface closure causing the cavity to continue to penetrate as suggested by Schwartz,[1] or whether the cavity ceases to penetrate after closure. However, in any event it is believed

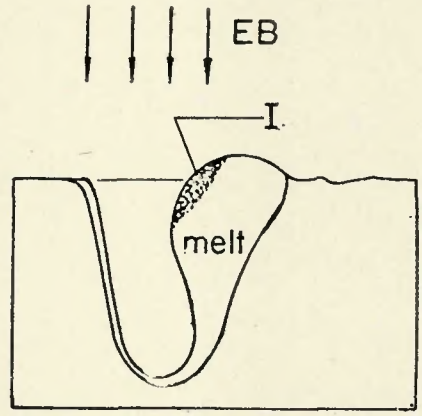

Fig. 7—Electron beam energy deposition—situation 1

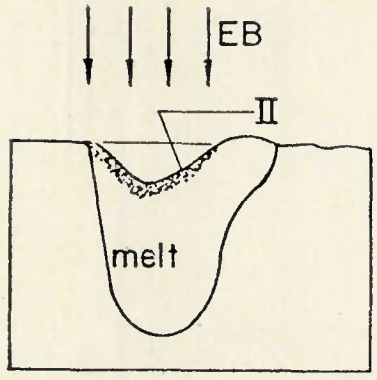

Fig. 8—Electron beam energy deposition—situation 2

that the surface closure or cap bursts due to an upward jet from a deep closure.

Deposition of Electron Beam Energy

For the conditions of the experiment, imagine then, that the cavity is in the shape shown in Fig. 4c. The deposition of electron beam energy at *I*, as shown in Fig. 7, causes a very high local vapor pressure which exerts a downward force on this portion of the melt. This force, combined with the forces due to surface tension and gravity, causes the melt to collapse into the cavity to give rise to the state shown in Fig. 4(d) and (e). Now the energy deposition is as shown in Fig. 8. Due to the large thickness of the fluid, region II attains a very high temperature which, in turn, causes a very high vapor pressure. This vapor pressure causes the cavity to penetrate once again giving rise to the shape shown in Fig. 4(b) where the cavity is shown at an intermediate depth and progresses subsequently to the configuration illustrated in Fig. 4(a) again. The process then repeats or oscillates.

The above model for the oscillation of the cavity adequately describes how some of the welding defects, observed in postweld macro-sections, are formed. A spike is formed each time the electron beam penetrates to the base of the weld and the severity of the spiking depends on the frequency of the oscillation and the welding speed

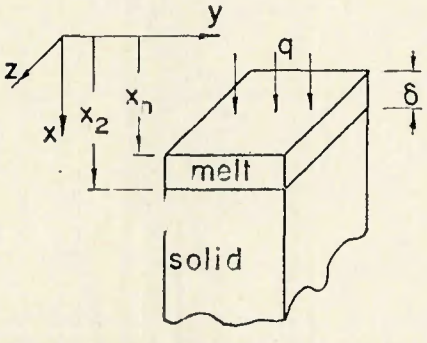

Fig. 10—Heat conduction at base of cavity

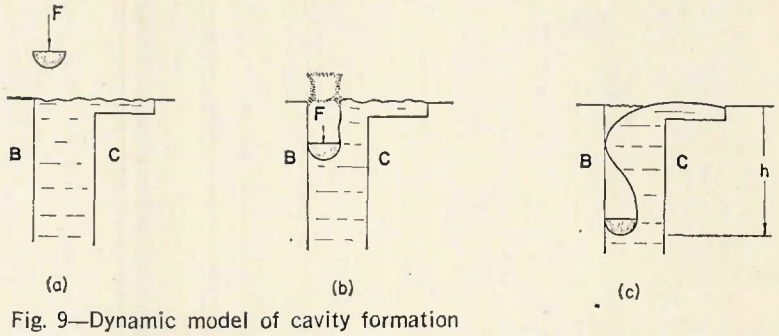

Fig. 9—Dynamic model of cavity formation

as well as the material being welded.

When the molten metal flows into the cavity, it can easily trap bubbles of contaminant gases at the base of the weld and, if the cooling rate is sufficiently rapid, the fluid may freeze before the gases can be convected to the surface, thus giving rise to porosity in the fusion zone. Similarly, if the cooling rate is sufficiently rapid, then the melt, as it falls into the cavity, may interrupt the beam long enough for the walls of the spike to freeze so that the fluid, upon falling into the spike, might not bond, thus forming a cold shut or crack.

The alternate penetration and closing of the cavity are also very efficient in mixing the melt and results in a very homogeneous fusion zone. The efficiency of this mixing is readily apparent from Fig. 3(b) where a local contaminant was spread through the complete depth of the weld. It is this feature that made it possible to delineate the relative size and shape of the molten region.

Cavity Oscillation Analysis

In a coordinate system fixed on the axis of the electron beam, the oscillation of the cavity is hypothesized to occur as shown in Fig. 9. The hemispheric body *A* is propelled downward by a force *F* into the fluid but its motion is constrained such that it is always very close to wall *B*. Upon impact a splash results and subsequently a cavity forms behind the sphere. The velocity of the body will decrease as its depth increases due to the retarding forces (surface tension, hydrostatic and dynamic forces). When the body has penetrated to a depth *h*, a deep closure occurs and separates the original cavity into a surface and subsurface cavity as shown in Fig. 9(c). The lower cavity then fills up; the upper cavity, however, may or may not fill completely. After a short time delay the fluid is struck by another body. The time delay is governed by the time required for the electron beam to develop a vapor pressure high enough to cause the cavity once again to penetrate.

The frequency of oscillation is primarily determined by the time required to penetrate to a depth *h* without any regard to how the closure is actually effected. This frequency can then be estimated by assuming that the cavity is a solid body of zero mass, forced to move through a fluid by the net force due to vapor pressure, surface tension and hydrostatic and dynamic forces. Such an analysis is given in Appendix I and the result is:

$$\frac{1}{2}\left[\frac{1}{f(A_1/A_2)}\,\frac{g}{h}\right]^{1/2}\tau = \left[\bar{p}_{ex}\right]^{1/2} - \left[\bar{p}_{ex} - 1\right]^{1/2} \qquad (1)$$

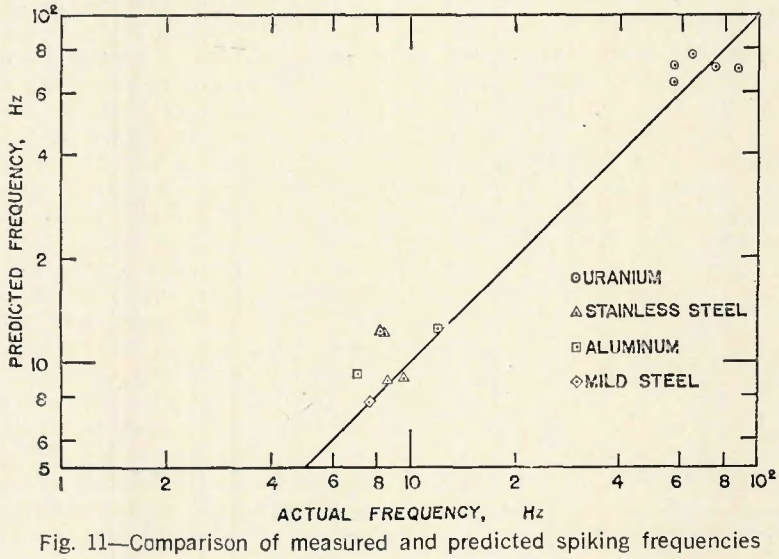

Fig. 11—Comparison of measured and predicted spiking frequencies

where τ is the time for the cavity to penetrate to the depth h and

$$\tilde{p}_{ex} = \left(p_v - \frac{2T_s}{a}\right)\frac{1}{\rho gh} = \frac{p_{ex}}{\rho gh} \quad (2)$$

$$f\left(\frac{A_1}{A_2}\right) = \frac{1}{2}\left(\frac{A_1}{A_2}\right)\left(1 + \frac{A_1}{A_2}\right) \quad (3)$$

The penetration velocity at an instant before closure of the cavity is (equation I-14):

$$\left.\frac{dx_n}{dt}\right|_{x_n = h} = \left[\frac{gh}{f(A_1/A_2)}\right]^{1/2} \left[\tilde{p}_{ex} - 1\right]^{1/2} \quad (4)$$

A qualitative interpretation of the dependence of τ on h can be provided by expanding eq (1) in a binomial series and rearranging to get:

$$\left[\frac{1}{f(A_1/A_2)}\right]^{1/2}$$

$$\tau \simeq h\sqrt{\frac{\rho}{p_{ex}}}\left[1 + \frac{gh}{4}\frac{\rho}{p_{ex}} + \ldots\right] \quad (5)$$

This shows that for given values of p_{ex} and $f\left(\frac{A_1}{A_2}\right)$, the penetration time is proportional to h in the lowest order approximation or the oscillation frequency is inversely proportional to the depth of penetration.

The frequency of the cavity oscillation, Hz, is related to τ and should be such that:

$$\text{Hz} \leq \frac{1}{\tau}$$

It has already been established that there is a delay between when the cavity closes and when the electron beam begins penetrating again. For lack of concrete evidence of the duration of this delay it shall be assumed that the delay is of the same order as τ so that:

$$\text{Hz} \approx \frac{1}{2\tau} \quad (6)$$

Experimental evidence (see Fig. 3) shows that the ratio of A_1 to A_2 is of order unity so that:

$$f\left(\frac{A_1}{A_2}\right) = \frac{1}{2}\left(\frac{A_1}{A_2}\right)\left(1 + \frac{A_1}{A_2}\right) \simeq 0^{\text{t}}$$

The oscillation frequency of the cavity, as determined above, represents the natural frequency of the cavity. A lower frequency, superimposed over the natural frequency, may occur due to an interaction of the static cavity closing forces (static head and surface tension) and the dynamic forces. The dynamic forces arise from the motion of the wave or ripple which is formed in the melt as the cavity penetrates. This ripple travels backwards along the surface of the melt and reflects off of the fused material. The reflected wave, upon arriving at the cavity, may force an early closure and hence a more complete filling of the cavity. This perturbation will affect the cooling and fusion rate of the melt as well as the time period for the subsequent cavity penetration. This will, in turn, be evident in the spiking pattern.

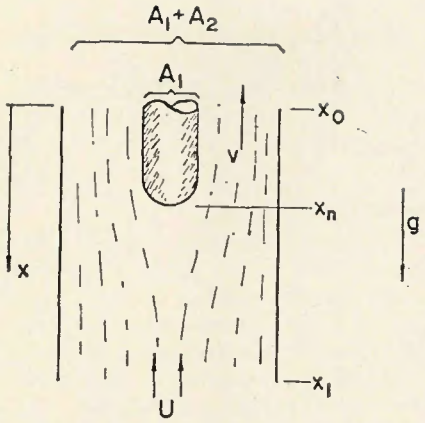

Fig. 12—Frictionless flow over an obstacle

The driving pressure p_{ex} is the net effect of surface tension and vapor pressure; the latter being a very sensitive function of temperature. The surface temperature, in turn, depends on the electron beam power and the transient motion of the melt which cannot be determined accurately with the present state-of-the-art. However, an approximate solution can be obtained if it is assumed that the vapor pressure remains nearly constant as the cavity penetrates and is determined by that pressure which exists at the base of the cavity an instant before closure. Since the penetration speed is usually much greater than the welding speed, the latter will be ignored so that the cavity penetration just before closure can be approximated by the one dimensional model shown in Fig. 10.

It will be assumed that the region δ is melt and the region $x > x_2$ is solid at the temperature T_m. When the cavity is almost at the maximum penetration depth, the electron beam is melting virgin material so that the thickness of the melt layer δ will be nearly constant. Then from Appendix II, the penetration velocity just before closure

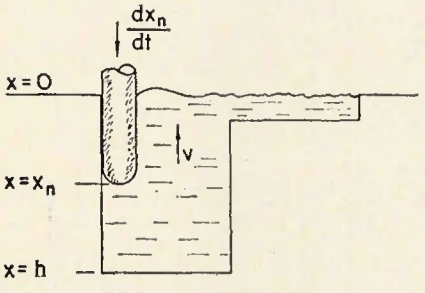

Fig. 13—Fluid flow over cavity

is given by:

$$\frac{dx_n}{dt} = \frac{4q}{\rho L}\left[2\left(\frac{q}{\rho L\alpha}\right)(\delta) + 3 + \sqrt{1 + 4\left(\frac{q}{\rho L\alpha}\right)(\delta)}\right]^{-1} \quad (7)$$

and the surface temperature of the melt is given by:

$$(T_n - T_m) = \left(\frac{\rho L\alpha}{k}\right)\left[-\frac{1}{4} + \frac{1}{4}\sqrt{1 + 4\left(\frac{q}{\rho L\alpha}\right)(\delta)} + \frac{1}{2}\frac{q}{\rho L\alpha}(\delta)\right] \quad (8)$$

Equations (7) and (8) can be represented by the nondimensional equations:

$$\frac{d\sigma_2}{d\tau} = 4\left[2\sigma_{2n} + 3 + \sqrt{1 + 4\sigma_{2n}}\right]^{-1} \quad (9)$$

and

$$\Gamma_n = \frac{1}{4}\left[-1 + 2\sigma_{2n} + \sqrt{1 + 4\sigma_{2n}}\right] \quad (9')$$

Further:

$$\frac{d\sigma_2}{d\tau} = [\Gamma_n + 1]^{-1} \quad (10)$$

where

$$\left.\begin{aligned} \sigma_2 &= \left(\frac{q}{\rho L\alpha}\right)x_2 \\ \sigma_{2n} &= \left(\frac{q}{\rho L\alpha}\right)(x_2 - x_n) \\ \tau &= \left(\frac{q}{\rho L\alpha}\right)^2 \alpha t \\ \Gamma_n &= \left(\frac{q}{\rho L\alpha}\right)\frac{k}{q}(T_n - T_m) \end{aligned}\right\} \quad (11)$$

The preceding solution for the oscillation frequency of the electron beam welding cavity was based on a combined fluid flow and heat transfer analysis. For a given externally applied force on the cavity, P_{ex}, the fluid flow analysis provided relationships for the cavity penetration time, τ, and the penetration velocity immediately prior to closure, $\left.\frac{dx_n}{dt}\right|_{x_n = h}$, as a function of the maximum penetration depth, h. The force, P_{ex}, is a function of the surface temperature of the melt, T_n, by virtue of the dependence of vapor pressure on temperature. The heat transfer analysis then provided the linking relationship between T_n and $\left.\frac{dx_n}{dt}\right|_{x_n = h}$. Thus for a given value of h and q the following iterative scheme can be used to calculate the cavity penetration time.

1. Assume a value of p_v such that:

$$p_v > 2\frac{T_s}{a} + \rho g h$$

2. Use this value in eq (4) to calculate $\left.\frac{dx_n}{dt}\right|_{x_n = h}$

3. Transform to the nondimensional quantity $\frac{d\sigma_2}{d\tau}$ and use eq (10) to get Γ_n and hence the surface temperature.

4. Determine the vapor pressure for this temperature from different sources[6–9] and compare this with the assumed value.

A solution, obtained with the above procedure, will yield not only the spiking frequency but also approximate values for the vapor pressure and surface temperature when the cavity is at its maximum depth.

Comparison of Oscillation Analysis with Experiments

Maximum definition of the spikes would be obtained for low spiking frequencies at high welding speeds so that the number of spikes per centimeter is low. This should result in very distinct spikes. Due to the low power (10 kw) of the welding unit used in the radiography experiments and its rather large spot size, deep welds (low frequencies) could only be obtained at low welding speeds. In spite of this, some welds on aluminum and steel with small scale spikes were analyzed and compared with the frequencies predicted by the previously described calculation procedure. The results are shown in Fig. 11 and tabulated in Table 1. In view of the many approximations incorporated in the analysis, the results are quite good. In these calculations, a spot diameter of 0.2 cm was used and it was assumed that:

$$\frac{A_1}{A_2} = 1$$

and that the cavity closing time was equal to its penetration time.

Additional data for welds on uranium* were analyzed and the results are also shown in Fig. 11. These uranium welds were made on a high voltage welding machine. ■

Conclusions

1. It has been shown by a radiographic technique, that the electron beam welding cavity oscillates with time. The time dependence of the shape of the cavity has been postulated to be analogous to the cavities formed by the entry of projectiles into water.

2. The oscillatory nature of the cavity provides an explanation for welding defects such as spiking, base metal porosity, and base metal cracking.

3. The oscillations also explain why the fusion zone is highly homogeneous. Making use of this homogeneity property, an experimental technique was developed to define the extent of the molten zone behind the cavity.

4. A dynamic model of the cavity oscillation was developed using the water entry phenomena and calculations of the spiking frequency were found to be within +6, −30% of the experimental values.

5. The fundamental difference between low and high voltage electron beam welding is believed to be the cavity closure mechanism. Low voltage welding gives rise to deep closures only and high voltage welding causes both surface and deep closures.

References

1. Schwartz, H., "Mechanism of High-Power-Density Electron Beam Penetration," J. Appl. Phys., 35, 7, pp. 2020-2029 (July 1964).

2. Wells, O. C., and Everhart, T. E., "A Note on the Physical Principles Underlying the Formation of the Cavity in Electron Beam Welding," 4th Annual Meeting Electron Beam Technology, Bakish, R. (ed.), pp. 105-122 (March 1962).

3. Tong, H., and Giedt, W. H., "Radiographs of the Electron Beam Welding Cavity," Review of Sci. Inst., (October 1969).

4. Mallock, A., "Sounds Produced by Drops Falling on Water," Proc. Royal Society London, Series A, Vol. 95 (November 7, 1918).

5. Gilbarg, D., and Anderson, R. A., "Influence of Atmospheric Pressure on the Phenomena Accompanying the Entry of Spheres Into Water," J. Appl. Phy. Vol. A19, No. 2 (February 1948).

6. Kohl, W. H., Handbook of Materials and Techniques for Vacuum Devices, Reinhold Pub. Corp., New York, N. Y., (1967).

7. Goldsmith, A., et al, Handbook of Thermophysical Properties of Solid Materials, Macmillan, New York, N. Y. (1961).

8. Dushman, S., Scientific Foundations of Vacuum Technique, John Wiley and Sons, New York, N. Y., (1949).

9. Honig, R. E., "Vapor Pressure Data for the Solid and Liquid Elements," RCA Review, 23, pp. 567-586 (December 1962).

10. Milne-Thomson, L. M., Theoretical Hydrodynamics, Maxmillan & Co., Ltd., London (1949).

11. Temple, G., Fluid Dynamics, Oxford University Press, (1958).

12. Goodman, T. R., "The Heat-Balance Integral and Its Application to Problems Involving a Change of Phase," Trans. ASME, Vol. 80, No. 2, pp. 335-342, (February 1958).

*Provided by Mr. R. E. Armstrong of the Lawrence Radiation Laboratory, Livermore, California.

Table 1—Spiking Results

Material	Power density, cal/sec-cm²	Depth of penetration, cm	Measured frequency, cps	Calculated Frequency, cps	T_{sur}, °K
Type 304 stainless steel	4.65×10^4	1.0	8.2	12.2	2560
	4.65×10^4	1.1	8.4	12.1	2560
	4.8×10^4	1.6	9.6	8.97	2570
	4.13×10^4	1.5	8.6	8.75	2568
AA 1100 aluminum	4.0×10^4	1.3	12.0	12.5	2100
	4.16×10^4	2.1	7.0	9.35	2131
Mild steel SAE 1018	4.0×10^4	1.7	7.6	7.69	2605
Uranium D-38	3.77×10^5	0.66	74.5	70.7	3706
	3.60×10^5	0.69	56.6	64.1	3700
	3.77×10^5	0.66	57.0	70.7	3706
	3.56×10^5	0.63	86.9	69.8	3690
	1.30×10^5	0.62	23.3	36.9	3480
	2.42×10^5	0.68	64.0	77.0	3756

Appendix

I. Cavity Development Analysis

Consider the steady flow of a bounded frictionless fluid around an obstacle as shown in Fig. 12. Let the cross-sectional area of the body be A_1 and the total cross-sectional area of the channel be $(A_1 + A_2)$. Then according to Bernoulli's equation, at any location in the fluid:

$$p - \rho g x + \frac{1}{2}\rho u^2 = \text{constant}$$

The potential energy term is negative because the positive coordinate direction has been taken as downward. Applying this equation at locations x_0 and x_1 gives:

$$p_1 = p_0 - \rho g(x_0 - x_1) + \frac{1}{2}\rho (v^2 - U^2) \qquad \text{(I-1)}$$

Conservation of mass requires that:

$$v = \left(1 + \frac{A_1}{A_2}\right) U \qquad \text{(I-2)}$$

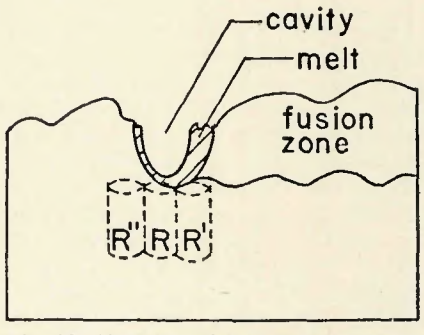

Fig. 14—Heat transfer at base of cavity

Let the volume of the body below x_0 be V and the reaction force of the body on the fluid be R (this is the negative of the drag on the body). Then applying Newton's second law to the fluid in the region bounded by x_0 and x_1:

$$R + p_0A_2 - p_1(A_1 + A_2) + \rho g\,[(A_1 + A_2)(x_1 - x_0) - V] = [\rho (A_1 + A_2)\, U]\,(U - v)$$

Substitution of eqs (I-1) and (I-2) into the above equation yields:

$$R = p_0A_1 + \frac{1}{2}\rho U^2A_1\frac{A_1}{A_2}\left(1 + \frac{A_1}{A_2}\right) + \rho g V$$

If $p_0 = 0$, then:

$$R = \frac{1}{2}\rho U^2A_1\left[\frac{A_1}{A_2}\left(1 + \frac{A_1}{A_2}\right)\right] + \rho g V$$

The volume of the body is given approximately by:

$$V \simeq A_1x_n$$

so that:

$$R = \frac{1}{2}\rho U^2A_1\left[\frac{A_1}{A_2}\left(1 + \frac{A_1}{A_2}\right)\right] + \rho g x_n A_1 \quad \text{(I-3)}$$

The force R is the reaction of the body on the fluid. The force of the fluid on the body, i.e. the total drag of the body is given by :

$$D = -\frac{1}{2}\rho U^2A_1\left[\frac{A_1}{A_2}\left(1 + \frac{A_1}{A_2}\right)\right] + \rho g x_n A_1 \quad \text{(I-4)}$$

The last term on the RHS of equation (I-4) is simply the buoyancy force and the first term is the drag due either to the motion of a fluid around a stationary body or to the motion of the body at velocity U through an initially stationary fluid.

Considering only the motion drag component, it is noted that the drag approaches infinity as A_2 approaches zero as one would expect for an incompressible fluid, but as A_2 approaches infinity, the drag approaches zero. This unexpected situation is a result of the inviscid flow assumption (and assuming $p_0 = 0$) and is known as D'Alembert's paradox[10, 11] which states that the drag, due to the motion of a finite body or a semi-infinite body with an asymptotic limit to its cross-sectional area, through an inviscid fluid, is zero.

Now consider the motion of a body through a confined fluid as shown in Fig. 13. A reservoir is provided near the top of the fluid so that $x = 0$ is approximately a fixed point independent of the depth of the body. If the body has a mass m_c and is subjected to an externally applied force $p_{ex}A_1$ in the positive x direction, then using eq (I-4) to approximate the retarding force, a force balance on the body yields:

$$\left\{p_{ex} - \left[\frac{1}{2}\rho U^2\left(\frac{A_1}{A_2}\right)\left(1 + \frac{A_1}{A_2}\right) + \rho g x_n\right]\right\}A_1 + m_c g = m_c\frac{d^2x_n}{dt^2}$$

The cavity formed by an electron beam is represented by a body of zero mass so that:

$$p_{ex} - \frac{1}{2}\rho U^2\left(\frac{A_1}{A_2}\right)\left(1 + \frac{A_1}{A_2}\right) - \rho g x_n = 0$$

and since $U = dx_n/dt$, then:

$$\left[\frac{1}{2}\left(\frac{A_1}{A_2}\right)\left(1 + \frac{A_1}{A_2}\right)\right]\rho\left(\frac{dx_n}{dt}\right)^2 + \rho g\, x_n = p_{ex} \quad \text{(I-6)}$$

This then is the approximate differential equation for the location of the base of the electron beam cavity. Examination of this equation shows that the cavity has an instantaneous velocity at $x_n = 0$ which is obviously not true. In fact, an additional term to account for the acceleration of the fluid (since dx_n/dt is not constant) should be included. This fluid acceleration term is estimated by potential flow theory (e.g., a source moving in a fluid of infinite extent) to be approximately:

$$\frac{7}{24}\rho a\frac{d^2x_n}{dt^2}A_1 \quad \text{(I-7)}$$

where $2a$ is the diameter of the body. The inclusion of this term would introduce a further complication in obtaining a solution for the motion of the electron beam cavity. It is for this reason that it is omitted but the possible error due to this omission was evaluated and found to be small.

An exact evaluation of the term.

$$\left[\frac{1}{2}\left(\frac{A_1}{A_2}\right)\left(1 + \frac{A_1}{A_2}\right)\right] = f\left(\frac{A_1}{A_2}\right)$$

would be extremely difficult in view of the current state of knowledge on electron beam welding. The experiments that were performed to estimate the extent of the melt region show that it is possible for A_1 to be greater than A_2, but generally of the same order of magnitude.

If we assume that p_{ex} is independent of x_n, then equation (I-6) can be solved as follows:

$$\left(\frac{dx_n}{dt}\right)^2 = \frac{1}{f(A_1/A_2)}\frac{p_{ex}}{\rho} - \frac{g}{f(A_1/A_2)}x_n \quad \text{(I-8)}$$

The RHS has the form $(a - bx_n)$ which will be denoted by n to give

$$\left(\frac{dn}{dt}\right)^2 = \left[\frac{g}{f(A_1/A_2)}\right]^2 n$$

or:

$$\frac{dn}{dt} = \pm\left[\frac{g}{f(A_1/A_2)}\right]\sqrt{n} \quad \text{(I-9)}$$

The boundary conditions are

$$t = 0 : x_n = 0$$

or

$$n = \frac{1}{f(A_1/A_2)}\frac{p_{ex}}{\rho}$$

$$t = \tau : x_n = h$$

or

$$n = \frac{1}{f(A_1/A_2)}\left(\frac{p_{ex}}{\rho} - gh\right) \quad \text{(I-10)}$$

where h is the maximum depth to which the cavity penetrates and τ is the time to penetrate to this depth. Integrating eq (I-9) and applying the boundary conditions gives, after some rearrangement

$$\pm\frac{1}{2}\left[\frac{1}{f(A_1/A_2)}\frac{g}{h}\right]^{1/2}\tau = \left[\frac{p_{ex}}{\rho gh} - 1\right]^{1/2} - \left[\frac{p_{ex}}{\rho gh}\right]^{1/2} \quad \text{(I-11)}$$

Since $\frac{p_{ex}}{\rho gh} \geq 1$, $\left[\frac{p_{ex}}{\rho gh} - 1\right]^{1/2}$ is always a real number and will be less than $\left[\frac{p_{ex}}{\rho gh}\right]^{1/2}$. In order that τ be positive, only the negative sign on the LHS is applicable so that:

$$\frac{1}{2}\left[\frac{1}{f(A_1/A_2)}\frac{g}{h}\right]^{1/2}\tau = \left[\frac{p_{ex}}{\rho gh}\right]^{1/2} - \left[\frac{p_{ex}}{\rho gh} - 1\right]^{1/2} \quad \text{(I-12)}$$

To determine the effective value of p_{ex}, consider the region where the external force is applied. There will be a positive force due to the vapor pressure of the molten metal and a negative force due to the surface tension. Therefore:

$$p_{ex}A_1 = p_vA_1 - 2\pi a\, T_s$$

where T_s is the surface tension or potential energy of the surface (units = force/length). Or,

$$p_{ex} = p_v - \frac{2T_s}{a} \quad \text{(I-13)}$$

The velocity at $x_n = h$ is obtained by taking the square root of eq (I-8) and evaluating it at $x_n = h$ to get:

$$\left.\frac{dx_n}{dt}\right|_{x_n = h} = \left[\frac{gh}{f(A_1/A_2)}\right]^{1/2}\left[\frac{p_{ex}}{\rho gh} - 1\right]^{1/2} \quad \text{(I-14)}$$

II. Surface Temperature at Base of Cavity

Consider the region at the base of the welding cavity just before closure occurs as shown in Fig. 14. The region

R can be modeled by a rectangular volume fixed in space with a constant heat input q and a constant melt layer thickness δ as shown in Fig. 10. It will be assumed that the solid is at a temperature T_∞ and that the heat transfer is one dimensional. In actual fact, the heat transfer is three dimensional and at any instant the solid will have been "preheated" while the cavity was over region R'.

There is a degree of compensation since the energy in the solid of region R due to preheating is approximately the same as the conduction loss from R to R''. The conduction loss in the z direction is slightly compensated for by using an average q whereas R should correspond to the region on the axis of the beam where the local heat input is greater than the average q. Note that although no melt removal mechanism is specified, it is implied that any melt in excess of the specified thickness δ is removed.

Let the reference temperature be the equilibrium melting temperature and define:

$$T' = T - T_m$$

Then the one dimensional transient heat conduction equation is:

$$\alpha \frac{\partial^2 T'}{\partial x^2} = \frac{\partial T'}{\partial t} \qquad \text{(II-1)}$$

and will be solved by an integral method first for the case of arbitrary motion of x_n and x_2 then reduced to the specific case of constant δ.

If (II-1) is multiplied by dx and integrated between the limits of x_1, and x_2, one gets:

$$\alpha \frac{\partial T'}{\partial x}(x_2, t) - \alpha \frac{\partial T'}{\partial x}(x_n, t) = T'(x_n, t)\frac{dx_n}{dt} + \frac{d}{dt}\int_{x_n}^{x_2} T'\,dx \qquad \text{(II-2)}$$

with the boundary conditions:

$$x = x_n : \frac{\partial T'}{\partial x}(x_n, t) = -\frac{q}{k} \qquad \text{(II-3)}$$

$$x = x_2 : T'(x_2, t) = 0 \qquad \text{(II-4)}$$

$$\frac{\partial T'}{\partial x}(x_2, t) = -\rho \frac{L}{k}\frac{dx_2}{dt} \qquad \text{(II-5)}$$

The last condition can be shown[12] to be equivalent to:

$$\left[\frac{\partial T'}{\partial x}(x_2, t)\right]^2 = \frac{\rho L \alpha}{k}\frac{\partial^2 T'}{\partial x^2}(x_2, t) \qquad \text{(II-5')}$$

Substitute conditions (II-3) and (II-5) into eq (II-2) to get:

$$\frac{q\alpha}{k} = T'(x_n, t)\frac{dx_1}{dt} + \frac{d}{dt}\left[\int_{x_n}^{x_2} T'(x, t)\,dx + \frac{\rho L \alpha}{k} x_2\right] \qquad \text{(II-6)}$$

Assume that the temperature distribution in the melt is given by:

$$T' = C_1(x - x_2) + C_2(x - x_2)^2$$

so that:

$$\frac{\partial T'}{\partial x} = C_1 + 2C_2(x - x_2)$$

$$\frac{\partial^2 T'}{\partial x^2} = 2C_2 \qquad \text{(II-7)}$$

Substituting these approximations into the boundary conditions (II-3) and (II-5'), C_1 and C_2 can be shown to be:

$$C_1 = \frac{\rho L \alpha}{2k\delta}\left\{1 - \sqrt{1 + \frac{4q}{\rho L \alpha}\,\delta}\right\}$$

$$C_2 = \frac{q}{2k\delta} + \frac{\rho L \alpha}{4k\delta^2}\left\{1 - \sqrt{1 + \frac{4q}{\rho L \alpha}\,\delta}\right\}$$

where the correct root was chosen in order to satisfy the physical situation. Defining:

$$\Gamma \equiv \left(\frac{k}{\rho L \alpha}\right) T'$$

$$\sigma \equiv \left(\frac{q}{\rho L \alpha}\right) x$$

$$\sigma_{2n} \equiv \sigma_2 - \sigma_n = \left(\frac{q}{\rho L \alpha}\right)\delta$$

$$\tau \equiv \left(\frac{q}{\rho L \alpha}\right)^2 \alpha t \qquad \text{(II-8)}$$

then the temperature distribution in the melt is given by:

$$\Gamma(\sigma, \tau) = \frac{1}{2\sigma_{2n}}\{1 - \sqrt{1 + 4\sigma_{2n}}\}\{\sigma - \sigma_2\} + \frac{1}{2\sigma_{2n}}\{\sigma - \sigma_2\}^2 + \frac{1}{4\sigma_{2n}^2}\{1 - \sqrt{1 - 4\sigma_{2n}}\}\{\sigma - \sigma_2\}^2 \qquad \text{(II-9)}$$

and in particular, the surface temperature is given by:

$$\Gamma(\sigma_n, \tau) = -\frac{1}{4} + \frac{1}{4}\sqrt{1 + 4\sigma_{2n}} + \frac{1}{2}\sigma_{2n} \qquad \text{(II-10)}$$

Similarly eq (II-6) can be written as:

$$1 = \Gamma(\sigma_n, \tau)\frac{d\sigma_n}{d\tau} + \frac{d}{d\tau}\left[\int_{\sigma_n}^{\sigma_2} \Gamma(\sigma, \tau)\,d\sigma + \sigma_2\right] \qquad \text{(II-6')}$$

Note that

$$\int_{\sigma_n}^{\sigma_2} \Gamma(\sigma, \tau)\,d\sigma = \int_{-\sigma_{2n}}^{0} \Gamma(\sigma - \sigma_2, \tau)\,d(\sigma - \sigma_2) = \frac{\sigma_{2n}}{6}\{\sigma_{2n} - 1 + \sqrt{1 + 4\sigma_{2n}}\} \qquad \text{(II-11)}$$

Substitute equations (II-11) and (II-10) into equation (II-6') and simplify to get:

$$1 - \frac{d}{d\tau}\left[\frac{\sigma_{2n}}{6}\left(\sigma_{2n} + 5 + \sqrt{1 + 4\sigma_{2n}}\right)\right] = \frac{1}{4}\left[2\sigma_{2n} + 3 + \sqrt{1 + 4\sigma_{2n}}\right]\frac{d\sigma_n}{d\tau} \qquad \text{(II-12)}$$

Note that up to this point, no restrictions have been placed on σ_n and σ_2. For a constant melt layer thickness i.e., σ_{2n} = constant, the derivative on the left hand side is zero so that:

$$\frac{d\sigma_n}{d\tau} = 4\left[2\sigma_{2n} + 3 + \sqrt{1 + 4\sigma_{2n}}\right]^{-1}, \quad \sigma_{2n} = \text{constant} \qquad \text{(II-13)}$$

and eq (II-10) is still valid for the surface temperature. In terms of the real variables, eqs (II-10) and (II-13) are respectively:

$$T_n = \left(\frac{\rho L \alpha}{k}\right)\left[-\frac{1}{4} + \frac{1}{4}\sqrt{1 + 4\frac{q}{\rho L \alpha}(x_2 - x_n)} + \frac{1}{2}\left(\frac{q}{\rho L \alpha}\right)(x_2 - x_n)\right] \qquad \text{(II-10')}$$

$$\frac{dx_n}{dt} = \frac{4q}{\rho L}\left[2\left(\frac{q}{\rho L \alpha}\right)(x_2 - x_n) + 3 + \sqrt{1 + 4\frac{q}{\rho L \alpha}(x_2 - x_n)}\right]^{-1} \qquad \text{(II-13')}$$